Detection of Defects in Glue Bonding of Cross-laminated Timber Using Experimental and Numerical Modal Analysis

Václav Sebera,* Patrik Nop, Jan Zlámal, David Děcký, and Marek Nociar

DOI: 10.15376/biores.21.2.4830-4853

* *Corresponding author: vaclav.sebera@mendelu.cz*

GRAPHICAL ABSTRACT

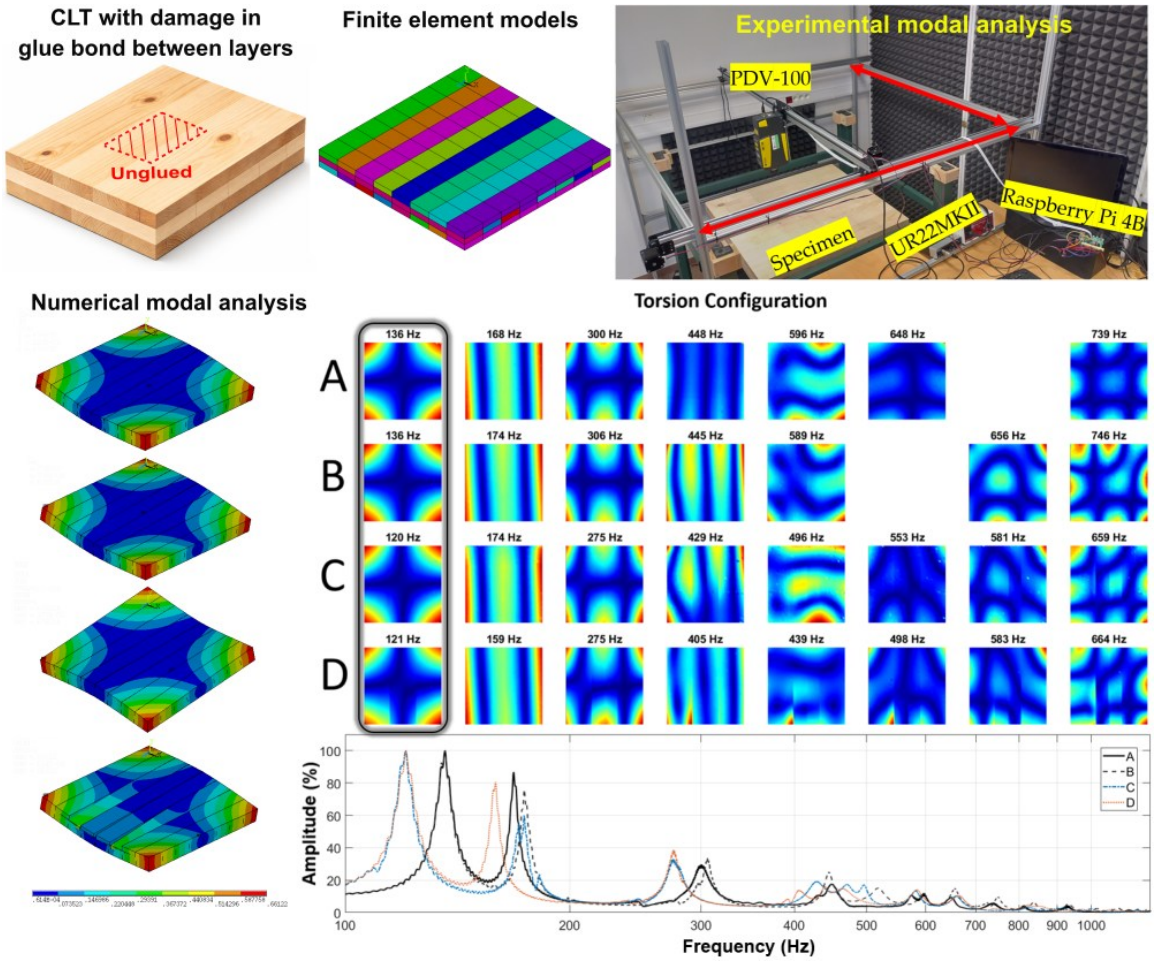

Detection of Defects in Glue Bonding of Cross-laminated Timber Using Experimental and Numerical Modal Analysis

Václav Sebera,* Patrik Nop, Jan Zlámal, David Děcký, and Marek Nociar

The preferred structural elements for taller timber buildings include cross-laminated timber (CLT), the performance of which significantly depends on the adhesive bond (AB) quality that may be influenced by manufacturing or factors within the service life. Both may contribute to a delamination, which represents a serious structural damage of the CLT. The study utilised both experimental and numerical modal analyses to assess the influence of damaged AB on CLT vibrational behavior. Both approaches confirmed that the CLT stiffness and eigenfrequencies decreased with AB damage, and both found agreement on certain modal shapes. FEA showed ideal patterns also in terms of localization of the damaged AB using modal shape damage index. Meanwhile, experiments showed its limits due to natural variability of wood, CLT, and measurement setup. The obtained results show a potential for *in situ* grading and inspection. However, the effect of variability of material properties of CLT should be studied further.

DOI: 10.15376/biores.21.2.4830-4853

Keywords: CLT; Adhesive bondline; Damage; Modal analysis; Spruce; Eigenfrequency; Damping; Finite element; Modal shape damage index

Contact information: Department of Wood Science and Technology, Faculty of Forestry and Wood Technology, Mendel University in Brno, Zemědělská 1665/1, Brno 61300, Czech Republic;
** Corresponding author: vaclav.sebera@mendelu.cz*

INTRODUCTION

Cross-laminated timber (CLT) is a massive timber material that is primarily used to build middle-to-tall timber buildings. The production and usage of CLTs in construction has increased worldwide due to their advantages, such as environment-friendliness and shorter time for assembly at construction sites (Brandner *et al*. 2016). The CLT panel is an engineered wood product whose layers are held by an adhesive. Such assembly assures that the material achieves compactness and structural performance. Therefore, the adhesive bonds play a crucial role in the CLT panel's mechanical and utility performance. The adhesive bonds may be corrupted either during the manufacture of the panel or during its service life within the structure. Therefore, a non-destructive test (NDT) procedure that is capable of uncovering damaged adhesive bonds within the CLT panel during service life or at the end of the manufacturing process is desired.

There are many NDTs one may use, but those based on ultrasound wave propagation or vibrations have an advantage because they are easy to carry out, relatively cheap, fast, and able to operate in an elastic range of deformations (Aicher and Dill-Langer 2008; Kurz and Boller 2015; Pahnabi *et al*. 2024). With respect to current study, one of the suitable techniques to find and locate damage (*e.g*. cavity, crack, decay) in a beam or panel

is modal analysis (MA), which has been used to analyze damage for several decades either implemented in finite element analysis (FEA) or experimental MA (EMA) (lrretier 2002; Brown and Allemang 2007; Shi *et al*. 2025). The MA provides eigenfrequencies and modal shapes that are strongly influenced by the presence of damage, since it modifies the distribution of stiffness and density within the volume of the panel when compared to undamaged scenarios. The MA provides a quality damage detection, especially when a damaged scenario (either physical or numerical) is compared to a sound one in terms of modal shapes and their derivatives.

For instance, Pandey *et al*. (1991) utilized MA and showed that damage in a beam modifies its eigenfrequencies. In addition, the location of the damage might be derived from the modal shape itself. The presence of a knot in a wooden beam represents a sort of damage and, therefore, it can also be found using the MA from flexural waves and curvatures, as shown in Yang *et al*. (2002, 2003) and Song *et al*. (2011). Choi *et al*. (2007) developed a modal-based damage-detection method to analyze simulated decay pockets in a timber beam. The authors found that the first two modes were enough to capture the extent and severity of damage using the modified damage index. Roohnia *et al*. (2011) successfully located a drilled hole in a defect-free beam by analysis of the shift of flexural modal frequencies if the hole is located away from the beam neutral axis. Similarly to timber beams, the MA is also suitable for the analysis of CLTs or other panels built in structures. These are usually examined at multiple points (grid), which enables visualisation of the natural modes. In particular, floor systems are often analyzed by MA, for instance in terms of their optimization with respect to design variables, their composition, and performance measures such as eigenfrequencies and damping (Weckendorf *et al*. 2016, Ussher *et al*. 2017). The MA may also be applied to floor systems built in constructions using experimental shakers and a set of accelerometers. Such an MA captures, to an advantage over pure lab tests, the interaction of the floors with constructions, since the boundary conditions *in situ* heavily influence dynamic behavior of CLT panels such as resonance, damping, and eigenfrequencies (Jarnerö *et al.* 2015; Faircloth *et al*. 2021; Kawrza *et al*. 2022). To analyze the structure, such as the CLT panel, it is advantageous to couple experimental and numerical approaches because it enables a deeper understanding of its dynamic behavior (Kawrza *et al*. 2021).

When carrying out MA of both sound and damaged scenarios, it is often needed to find equivalent modes (mode pairing) between them, as the damage in the structure will give rise to new modes that do not exist in sound scenarios. For that purpose, there are several metrics, among which the modal assurance criterion (MAC) and its derivatives are most commonly used (Allemang 2003). The MAC, which expresses a sort of correlation among modes, may also be used to pair modes obtained from FEA and EMA, as was demonstrated for timber beams in Kouroussis *et al*. (2017a,b). More recently, Bondsman and Peplow (2025) reported on beams cut out of CLT that their modal performance shows high variability in resonance frequencies, modal damping, and vibration transfer function, especially for torsional modes, due to the variability of the material. When material properties of CLT are not known, an inverse methodology utilizing MA outputs may provide them when an objective function is well stated (Bondsman and Peplow (2024).

Once the modes and eigenfrequencies are paired, the damage may be localized from the postprocessing of modal shapes, for instance, using modal shape damage index (MSDI), modal strain energy, or others (Wang and Chan 2009; Samali *et al*. 2010; Duvnjak *et al*. 2016; Li *et al*. 2023). For plate-like structures, these indices allowed the finding of damage based on computed or measured modal displacements and strains, as was shown

for concrete and sandwich panels (Meruane *et al*. 2017; Duvnjak *et al*. 2021). It is hypothesized that damage in adhesive bonding inside the CLT panels may be detectable using such indices based on data from experimental and numerical MA.

Therefore, the specific objectives of the research were: 1) to manufacture CLT panels made of spruce with and without imperfections in bonding; 2) to perform experimental modal analysis of manufactured CLTs with simple-support boundary conditions using semiautomatic system employing the laser doppler vibrometer (LDV); 3) to perform data analysis from LDV about eigen frequencies and damping; 4) to carry out the finite element modal analysis of various scenarios in bonding to obtain eigenfrequencies and modal shapes, and to find equivalent modes among designed scenarios using MAC; and 5) to localize damage in bonding between layers using MSDI.

MATERIALS AND METHODS

Material Preparation

Tested specimens consisted of four three-layered cross-laminated timber (CLT) panels made of Norway spruce (*Picea abies*). The layer had a thickness of 27 mm, so the total size of the panel was 800 x 800 x 81 mm³. Each CLT panel was different in terms of its adhesive bond. The following gluing scenarios were produced: A - CLT panel was glued without an imperfection in AB; B - CLT panel was glued with an imperfection of 10% of total panel in the center of the panel; C - CLT panel was glued with an imperfection of 40% of total panel area in the center of the panel; D - CLT panel was glued with an imperfection of 40% of total panel area at the side of the panel (Fig. 1).

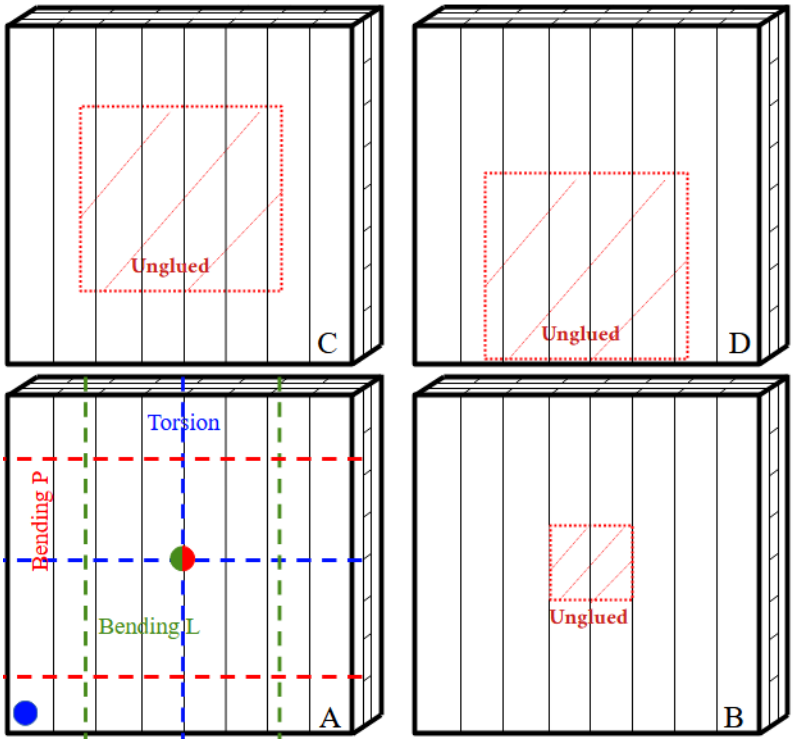

Fig. 1. Sketch of designed CLT damage scenarios A, B, C and D with boundary conditions (BCs) distinguished with colored dashed lines (torsion is blue, BendingL is green, BendingP is red), the circle represent place where shaker was attached to CLT for particular BCs.

The boards in neither CLT panel were glued edge-wise, and the imperfection in AB was introduced only between the top and the middle layer. The polyurethane glue PUR 2010 (AKZONOBEL) was used for the production of all CLT panels with glue spread rate of 180 g/m^2 and a manufacturing pressure of ~ 0.8 MPa.

The moisture content (MC) of the CLT panels prior to MA was measured using a dielectric moisture meter (Orion Wagner L601) 10 times from each side of the panel, so the resulting MC of the panel is expressed as the mean value from 20 measurements (Table 1). Before measurement, the global density of the CLT panels was also calculated as the weight of the panel divided by its nominal volume (Table 1).

Table 1. Moisture Content and Global Density of the CLT Panels during Measurement (CV - coefficient of variation, in brackets)

Scenario	A	B	C	D
Mean MC (CV) [%]	9.11 (9.27)	8.47 (9.43)	8.30 (15.28)	8.98 (10.89)
Global density [kg/m^3]	483	476	468	431

Numerical Modal Analysis

For performing all numerical modal analyses of CLT panels, the software used was Ansys 21R2 (Ansys Inc., USA). The FE models of CLT were created based on physical CLT scenarios (A, B, C, D), and one extra was created (A+). The scenario A+ represents a CLT panel that is glued not only between layers, but also within the layer, so it represents the stiffest scenario simulated. The FE models were built using a top-down approach by quadratic solid finite elements (FE) SOLID185. In total, the FE models had about 58k of FE's and 86k nodes (Fig. 2). The boundary conditions mimicked the experimental modal analysis setup, so all the FE models were constrained in a way that nodes at the bottom of CLTs at certain locations were simply supported (see Fig. 1). This reflected supporting the CLT panel during experimental modal analysis on elastic ropes at the location of vibrational nodes. The material properties of spruce used in all FE models were linear elastic orthotropic.

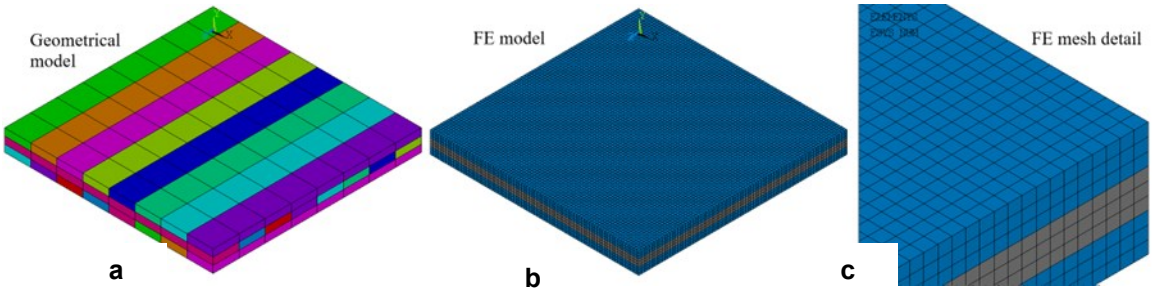

Fig. 2. a) Geometrical model of CLT with colored distinction of lamellae; b) Whole FE mesh of CLT panel and c) Detail of the FE mesh

The material properties were taken from Požgaj *et al.* (1993) because it was based on materials grown in the same region (Czechia and Slovakia) as in the present work. The properties were as follows: ρ = 450 kg.m^{-3}, E_L = 13.65 GPa, E_R = 0.789 GPa, E_T = 0.289 GPa, G_{LR} = 0.474 GPa, G_{RT} = 0.573 GPa, G_{LT} = 0.289 GPa, μ_{LR} = 0.014 GPa, μ_{RT} = 0.557

GPa, μ_{LT} = 0.014 GPa, where E is the normal elastic modulus, G is the shear modulus, and μ_{ij} is Poisson's ratio, and indices L, R and T stand for wood anatomical directions longitudinal, radial and tangential, respectively.

The imperfection in glueing was made by not joining the FE nodes of adjacent layers (boards). Therefore, the reference scenarios (A and A+) had only one node at the location shared by two elements from different layers, but scenarios with imperfection had two nodes at the same location and without any interaction between them (no contact was defined). The Block-Lanzcos solver for all analyses was used, and frequencies up to 800 Hz for all panels were investigated. However, each scenario had a different number of modes computed up to 800 Hz due to imperfections. Therefore, to find equivalent natural frequencies and modal shapes compared to the reference scenario (A), the modal assurance criterion (MAC) with a threshold of 0.3 was employed. Consequently, the MAC made it possible to sort modal shapes and natural frequencies and enabled a tool to compare them also to outputs of experimental modal analysis. Once modal shapes were obtained, relative displacement fields of all scenarios from the surface of the panels were extracted. Then, from the extracted modal displacements, the modal shape damage index (MSDI) was calculated between reference scenario and scenarios with damaged AB. The MSDI was used to investigate whether the damaged glue bondline inside the CLT panel is detectable from surface modal shape data. The MSDI was calculated using Eq. 1,

$$MSDI = \left(\frac{\varphi_u - \varphi_d}{\varphi_u}\right) * 100 \quad (1)$$

where φ denotes modal displacement, indices u and d stand for undamaged and damaged scenarios, respectively. All the post finite-element calculations and statistics were performed in Matlab 2024R1 (Mathworks, USA).

Experimental Modal Analysis

The EMA approach was used to determine the plane dynamic response of the entire specimens. Each specimen was tested in three configurations, corresponding to three fundamental plane vibration modal shapes (Fig. 1). In each configuration, the specimen was supported by flexible ropes at the nodal lines. For the torsional mode configuration, the ropes crossed the specimen perpendicularly at 50% of its length, with the dynamic force applied at one corner (blue lines in Fig. 1a). For the longitudinal bending ($Bending_L$) and the perpendicular bending ($Bending_P$) mode configurations, the nodal lines were located at 22.4% and 77.6% of the specimen length, with the dynamic load applied at the center (red and green lines at Fig. 1a).

The dynamic load was applied using a dynamic shaker GW-V20 (DataPhysics Instruments GmbH, Filderstadt, Germany) connected *via* epoxy-bonded nuts placed at the antinodes of the fundamental modal shapes (Fig 1). The excitation signal was a looped logarithmic sine sweep in the frequency range of 50 to 5000 Hz. Specimen vibrations were measured using a PDV-100 laser vibrometer (Polytec GmbH, Waldbronn, Germany) over a 51 × 51 - point grid, with spacing between individual points set to 2% of the specimen's side length. Measured signals were recorded using a Steinberg UR22MKII external sound card (Steinberg Media Technologies GmbH, Hamburg, Germany) at a sampling frequency of 44.1 kHz. The synchronisation of excitation, data acquisition, and the control of stepper motors moving the vibrometer in two axes along the assembled frame was ensured using a Raspberry Pi 4B system (Raspberry Pi Holdings Ltd., Cambridge, UK) (Fig. 3). For all scenarios with imperfections, measurements were taken from the layer where the

imperfections were located. To improve the laser vibrometer signal-to-noise ratio, a reflective aluminium adhesive foil was added to the measured specimen surface.

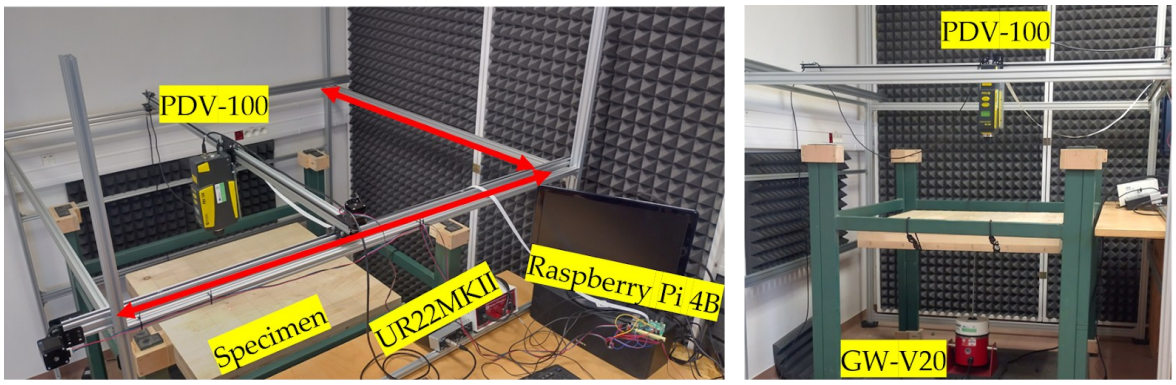

Fig. 3. The setup used for experimental modal analysis. The red arrows indicate the movement of vibrometer at the testing frame.

Experimental Data Analysis

All tasks related to signal processing and data evaluation were carried out in the MATLAB environment (MathWorks, Natick, USA). A Fast Fourier Transform (FFT) was performed on the signal from each measured point. The frequency spectrum of the entire specimen was created as the mean of the spectra of all measured points. To identify the modal shapes corresponding to the frequency peaks in the spectrum, the amplitudes of individual points at resonance frequencies were visualised. The dynamic shear elastic modulus (G_{dyn}) was determined using the frequency of the torsional modal shape according to Eq. 2,

$$G_{dyn(n)} = \frac{4lmf_{T,n}^2}{bt} R \quad (2)$$

where l is the length of the specimen (m), m is the mass of the specimen (kg), n is the order of the torsional mode (n=1), b is the width of the specimen (m), t is the thickness of the specimen (m), and R is a correction factor expressed by Eq. 3.

$$R = \left[\frac{1+\left(\frac{b}{t}\right)^2}{4-2.521\frac{t}{b}\left(1-\frac{1.991}{e^{\pi\frac{b}{t}}+1}\right)}\right]\left[\frac{1+0.00851n^2b^2}{l^2}\right] + 0.06\left(\frac{nb}{l}\right)^{\frac{3}{2}}\left(\frac{b}{t}-1\right)^2 \quad (3)$$

The MOED was calculated from the bending mode frequency (f_B) using Eq. 4,

$$MOED = \frac{4\pi^2 f_{B,n}^2 l^4 \rho}{\beta^4 i^2} \quad (4)$$

where β is a constant corresponding to the mode order (β = 4.73 for n = 1), and i is the radius of gyration, calculated using Eq. 5.

$$i = \frac{t}{\sqrt{12}} \quad (5)$$

The damping ratio (ζ) of each observed modal shape was estimated using the half-power method. At the amplitude level of $1/\sqrt{2}$ of the frequency peak (f), the corresponding

lower (f_l) and upper (f_u) frequencies were determined. The value of ζ was calculated using Eq. 6.

$$\varsigma = \frac{f_u - f_l}{2f} \quad (6)$$

RESULTS AND DISCUSSION

Numerical Analysis

The numerical MAs were carried out for all the scenarios up to 800 Hz and for all three configurations. Their outputs are first plotted as frequency *vs.* mode number paths (Fig. 4). The figure shows modes before mode matching, so it does not show frequencies at equivalent modes. However, these paths are a good illustration of the fact that the damage in adhesive bonds (AB) introduced new eigenfrequencies (modes) that did not occur for sound and reference scenarios (A or A+). These frequency-mode paths start to differ for damaged scenarios from the reference one at certain bifurcation points. The greater the extent of the AB damage, the earlier this point appears in the diagram. Further, the damage in AB decreases the eigenfrequencies due to the reduction of stiffness caused by the missing adhesive. The defectless scenarios A and A+ show very parallel paths, and because A is less stiff, its eigenfrequency paths are slightly below the paths for scenario A+.

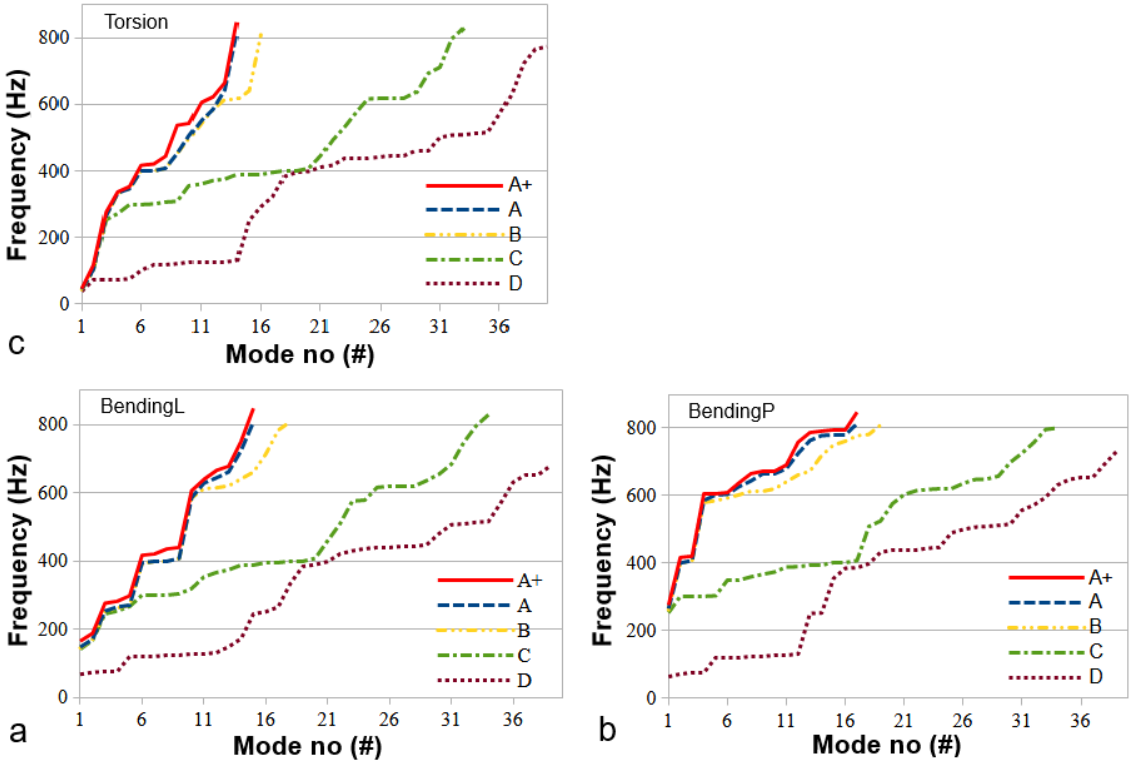

Fig. 4. Frequency vs. mode number paths obtained from numerical MA for three configurations: a) Bending$_L$, b) Bending$_P$, and c) Torsion

Scenario B started to differ from A and A+ at all BCs around 600 Hz; meanwhile, severe damages in AB (scenario C primarily) started bifurcating much earlier, or they had a unique path (scenario D). The damage in AB at the side (scenario D) represented the least stiff scenario and had the lowest eigenfrequencies. This means that if debonding of

lamellae occurred at the side, the impact to the vibrational and structural performance of CLT was higher than when it occurred in the middle of the CLT, for instance, due to errors in manufacture. From Fig. 4, it is visible that for damaged scenarios, there were many new modes with very similar eigenfrequencies that did not exist for sound scenarios. These conjugated frequencies appeared as horizontal-like ranges in Fig. 4 and represented modes of vibration of loose lamellae. Their vibrations lay in a plane of the CLT panel, and examples of such conjugated eigenfrequencies may be seen in Fig. 5a, 5b and 5c.

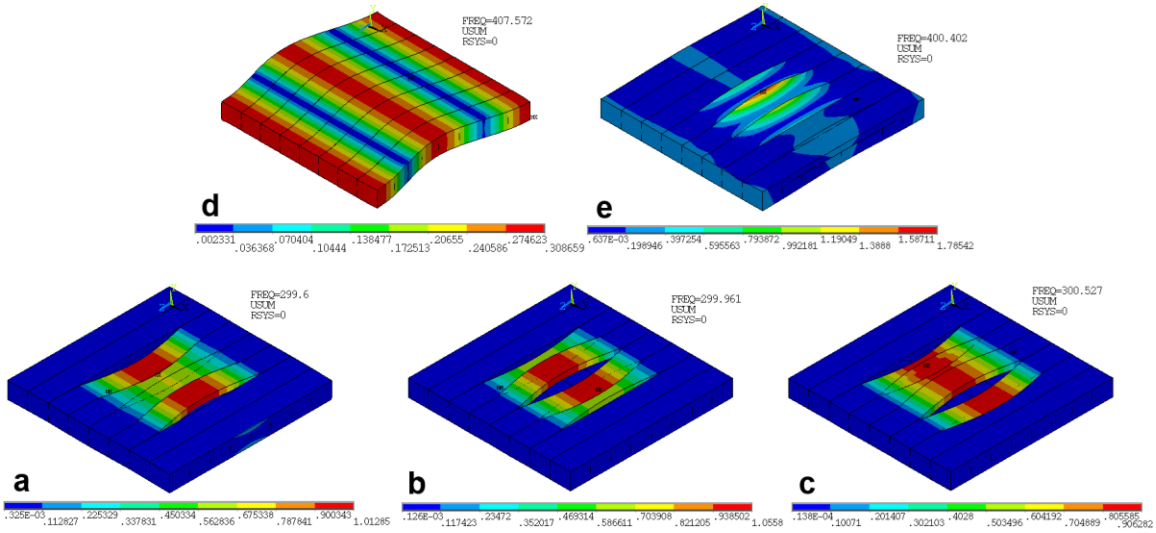

Fig. 5. a), b) and c) represent conjugated new modes that occur due to damage in AB (scenario C; d) and e) represent modes of scenario A (8th mode) and C (18st mode) in torsion configuration paired on a basis of MAC = 0.60.

The eigenfrequencies that represent the vibrations of loose lamellae make the situation of comparing particular scenarios between each other more difficult. For that reason, MAC was used to find equivalent modes amongst different scenarios at a certain configuration. For successful mode pairing, MAC values should be as high as possible to assure high-quality matching. It is generally recommended to have MAC higher than 0.7. However, in this case, the damage in AB was so severe for scenarios C and D that the modal shapes were changed substantially. Therefore, the minimal MAC was set to be 0.3, and then paired modes with low MAC values (0.3 to 0.5) were investigated carefully, and also visually. The MAC value above 0.5 did not guarantee correct matching. This was apparent from Figs. 5d and 5e, which show matched modes (8th in A scenario and 18th in C scenario) with MAC = 0.60. The outputs of mode matching using MAC for the first 15 modes are shown in Tables 2, 3 and 4 for Bending$_L$, Bending$_P$, and Torsion, respectively. Tables 2, 3 and 4 contain sequences of data for each scenario as: mode number, eigenfrequency (in Hz), relative frequency difference (in %) and MAC (unitless), so it enables to learn to what extent the damage in AB alters the vibration modes.

From the Tables 2, 3 and 4, the following observations may be drawn: (i) for equivalent modes, the eigenfrequency decreased as the damage in AB increased, although there were a few exceptions given by matching with low MAC; (ii) the minimal MAC value within 15th studied modes decreased as damage in AB increased (the same was observed for mean MAC); (iii) the correlation coefficients (R) between MAC and relative difference of frequency with respect to scenario A decreased with increase of damage and they ranged from -0.87 to 0.14, which implies that MAC may be one of the indicators of

damage; however, non-negligible uncertainties should be kept in mind; (iv) mean relative difference of paired eigenfrequencies (mRD) with respect to scenario A increased with increase of damage of AB for studied 15 modes; (v) the reference scenario A with respect to scenario A+ actually behaved as a defect in gluing with similar mRD as found between A and C for instance; this implies that the effect of gluing boards by sides resulted in substantial change in eigenfrequencies, especially for first 7 modes; (vi) for bending configurations, damage in D was so severe that a few modes did not occur at all.

Table 2. FEM-computed Eigenfrequencies for the First 15 Equivalent Modes with Respect to Reference Scenario A in Bending$_L$ Configuration.

A fem	A+ fem	B fem	C fem	D fem
Mode no. [#] / Frequency [Hz] / Frequency difference [%] / MAC [-]				
1/147	1/165/12/1.0	1/145/1.3/1.0	1/141/4.1/1.0	13/148/0.7/0.87
2/170	2/187/10/1.0	2/170/0.2/1.0	2/167/1.8/1.0	14/172/1/0.90
3/253	4/276/11/1.0	3/252/0.3/1.0	3/245/3.3/1.0	15/245/3.3/0.95
4/265	3/282/4.0/1.0	4/262/1.1/1.0	4/253/4.6/1.0	16/251/5.4/0.99
5/270	5/298/10/1.0	5/270/0/1.0	5/266/1.3/1.0	17/265/1.9/0.95
6/394	8/417/10/1.0	6/391/0.8/1.0	10/319/19.2/0.51	20/389/1.4/0.49
7/400	9/420/10/0.93	8/400/0/0.99	16/393/6.4/0.98	23/429/7.4/0.54
8/400	6/435/4.1/0.93	7/399/0.3/0.99	14/388/3.0/0.99	19/389/4.1/0.95
9/ 408	7/440/3.1/1.0	9/407/0.1/1.0	18/400/1.8/0.61	21/398/2.4/0.95
10/585	10/606/3.4/0.99	10/585/0.1/1.0	23/575/1.7/0.99	35/571/2.5/0.97
11/628	11/639/1.7/1.0	13/620/1.3/0.94	22/509/19/0.67	18/335/46.7/0.40
12/643	12/665/3.4/0.99	14/641/0.4/1.0	29/636/1.2/0.97	36/631/1.9/0.97
13/661	13/678/2.5/1.0	15/660/0.1/1.0	30/654/1.1/0.99	37/650/1.6/0.97
14/724	14/751/3.7/1.0	16/713/1.4/0.98	31/684/5.6/0.70	39/679/6.2/0.59
15/808	17/847/9.7/0.99	17/783/3.0/0.91	35/845/4.6/0.62	Not present
mRD [%]	5.5	0.5	5.2	5.8
minMAC [-]	0.93	0.91	0.51	0.4
R [-]	0.02	-0.8	-0.67	-0.49

Note: mRD denotes mean relative difference in frequency for all 15 modes, minMAC denotes the minimal MAC value in the set, and *R* is correlation coefficient between frequency difference and MAC.

The modal shapes (summed modal displacement vector) of the first 15 modes shown in Tables 2, 3 and 4 are attached as supplemental materials S1, S2 and S3, respectively, and they are also aligned with respect to scenario A. Looking at the S1, S2, and S3, one may make following conclusions: a vast majority of modal shapes of damaged scenarios B, C and D were matched with modal shapes of A (A+ also), although there were a few cases where even visually the modal shape looked different. For instance: (ii) in configuration bending$_L$ (see S1), it was mode no. 6 and 9 of scenarios C and D; (ii) in

configuration bending$_P$, it was mode no. 3, 5, 6, 12, and 15 of scenarios C and D (see S2), and (iii) in configuration torsion, it was mode no. 8 and 14 (see S3). At this stage, the first 15 modes were evaluated, no matter whether they had significant modal displacement perpendicular to CLT, which is important for the experimental part because this component was measured.

Table 3. FEM-computed Eigenfrequencies for the First 15 Equivalent Modes with Respect to Reference Scenario A in Bending$_P$ Configuration

A fem	A+ fem	B fem	C fem	D fem
Mode no. [#] / Frequency [Hz] / Frequency difference [%] / MAC [-]				
1/265	1/276/4/1.0	1/262/1.1/1.0	1/253/4.1/1.0	13/251/5.4/0.99
2/400	2/417/4.1/1.0	2/399/0.3/1.0	11/389/1.8/0.99	16/384/3.9/0.95
3/407	3/420/3.1/1.0	3/407/0.1/1.0	15/400/3.3/0.604	18/398/2.4/0.95
4/585	4/606/3.4/1.0	5/585/0.1/1.0	20/576/4.6/0.98	32/572/2.3/0.91
5/602	5/607/0.8/1.0	6/593/1.5/0.89	14/396/1.3/0.41	14/253/58/0.55
6/604	6/609/0.9/1.0	7/602/0.2/0.94	19/525/19.2/0.58	25/489/18.9/0.32
7/627	7/638/1.8/1.0	10/620/1.1/0.80	21/603/6.4/0.55	33/595/5.2/0.55
8/643	8/665/3.4/0.99	11/641/0.4/1.0	26/636/3.0/0.96	34/631/1.9/0.97
9/664	9/671/1.1/1.0	12/661/0.4/0.99	18/508/1.8/0.51	38/693/4.4/0.46
10/664	10/672/1.2/1.0	4/580/12.7/0.52	6/348/1.7/0.59	37/653/1.6/0.37
11/679	11/691/1.7/1.0	13/672/1.1/0.57	27/647/19/0.59	Not present
12/725	12/758/4.6/1.0	14/719/0.8/0.98	28/649/1.2/0.38	36/652/10/0.52
13/763	15/793/4/1.0	15/750/1.7/0.99	30/698/1.1/0.52	39/730/4.3/0.36
14/778	13/787/1.2/1.0	17/777/0.1/1.0	31/725/5.6/0.42	Not present
15/781	16/793/1.6/0.71	16/761/2.6/0.98	29/658/4.6/0.64	35/647/17.1/0.42
mRD [%]	2.5	1.6	12	9.6
minMAC [-]	0.71	0.52	0.38	0.32
R	0.17	-0.7	-0.43	-0.25

Notes: The term mRD denotes mean relative difference in frequency for all 15 modes, minMAC denotes the minimal MAC value in the set, and R is correlation coefficient between frequency difference and MAC.

Experimental Analysis

The EMA provided several outputs. First, using equations 1 to 5 made it possible to obtain fundamental material properties such as dynamic moduli of CLTs in given scenarios. The frequencies used for the calculation of dynamic moduli were selected according to the associated measurement configuration (torsional for torsion, etc.), and the results are shown in Table 5. From the table, one may see that properties differed substantially amongst scenarios: (i) the value of G_{dyn} was lower for scenario B by 1.3%, for C by 23.9% and for D by 29.9%; (ii) $MOED_L$ was higher for B by 4.9%, for C it was higher by 1.9%, and for D it was lower by 21.7%; (iii) $MOED_T$ was lower for B by 7.5%, for C by 31.6%, and for D by 48.0%. Theoretically speaking, all stiffnesses of the CLTs tended to decrease as the damage in AB increased, which was clearly apparent for G_{dyn} and

$MOED_T$. The opposite tendencies shown in Table 5 for $MOED_L$ may be attributed to the variability of wood stiffness and mass within lamellae and within the CLT panels, and, lastly, to measurement inaccuracies (discussed further).

Table 4. FEM-computed Eigenfrequencies for the First 15 Equivalent Modes with Respect to Reference Scenario A in Torsion Configuration

A fem	A+ fem	B fem	C fem	D fem
Mode no. [#] / Frequency [Hz] / Frequency difference [%] / MAC [-]				
1/44	1/46/5.2/1.0	1/43.6/0.5/1.0	1/42.5/3.1/1.0	1/37.8/13.7/0.98
2/103	2/116/12.8/1.0	2/103/0.2/1.0	2/101/1.6/1.0	6/99.8/3.2/0.90
3/265	3/276/4/1.0	3/262/1.1/1.0	3/253/4.5/1.0	15/251/5.3/0.99
4/334	4/337/0.9/1.0	4/333/0.4/1.0	4/272/18.7/0.62	16/292/12.6/0.91
5/346	5/353/1.9/1.0	5/346/0.1/1.0	9/308/11/0.4	17/322/6.9/0.96
6/398	8/444/11.4/1.0	6/398/0.1/1.0	15/390/2.1/0.99	19/396/0.7/0.61
7/400	6/417/4.1/1.0	7/399/0.3/1.0	14/388/3/0.99	18/384/4.1/0.97
8/408	7/420/3.1/1.0	8/407/0.1/1.0	18/400/1.9/0.61	20/398/2.3/0.87
9/452	9/537/18.7/0.99	9/452/0.1/1.0	21/444/1.8/0.99	29/459/1.6/0.86
10/505	10/542/7.3/1.0	10/500/1.7/0.99	22/493/2.5/0.78	30/460/9/0.86
11/551	12/622/13/0.99	11/542/1.6/0.99	23/531/3.6/0.83	31/501/9.2/0.82
12/585	11/606/3.4/0.99	12/585/0.1/1.0	24/575/1.7/0.98	36/571/2.5/0.97
13/643	13/665/3.4/0.99	15/641/0.4/1.0	29/636/1.2/0.96	37/631/1.9/0.97
14/813	14/847/4.2/0.99	16/809/0.5/1.0	32/796/2.1/0.99	40/773/4.9/0.50
15/833	15/851/2.3/0.99	17/831/0.2/1.0	33/829/0.5/1.0	47/826/0.8/0.99
mRD [%]	6.4	0.5	4	5.2
minMAC [-]	0.99	0.99	0.4	0.5
R [-]	0.12	-0.87	-0.65	0.14

Note: The term mRD denotes mean relative difference in frequency for all 15 modes, minMAC denotes the minimal MAC value in the set, and R is correlation coefficient between frequency difference and MAC.

Table 5. Non-destructively Determined Physical–mechanical Properties of Tested Specimens (scenarios A–D)

Scenario	ρ (kg·m^3)	G_{dyn} (MPa)	$MOED_L$ (MPa)	$MOED_T$ (MPa)
A	483	467.7	750.8	8841.3
B	476	459.7	790	8142
C	468	354.4	765	5965
D	431	327.9	589.3	4557.7

Second, the EMA provided frequency spectra, eigenfrequencies, and vibrational modal shapes (eigenfrequencies below 50 Hz were not measured). The frequency spectra and vibrational modal shapes for all scenarios and configurations are shown in Figs. 6, 7, and 8, where nodes are shown in blue, while antinodes are depicted in colours ranging from yellow to red. In general, the torsional configuration (Fig. 6) shows that the eigenfrequency of CLTs decreased as damage in AB increased, although there were discrepancies, as shown for scenarios B and C. These discrepancies may be attributed to natural variability of wood and measurement inaccuracies. For scenario B, one may also say that the damage in AB likely did not have an impact on vibrational behavior to the extent that would outbalance other effects, so several eigenfrequencies were higher than for scenario A (note lower or similar eigenfrequencies for B scenario in Fig. 6 and Table 4). The measurement inaccuracies come from the fact that each CLT has a different mass distribution within its volume and, furthermore, due to attachment to the shaker, each CLT might experience slight movement on supports during measurement, which intensifies the effect of mass nonuniformity. Although the intended setup tried to minimize this effect, in fact, it is inevitable for materials such as CLT to a certain degree when using such a setup. From Fig. 6, one may observe that the damage in AB was not clearly visible from the modal shapes for scenario B, but for scenarios C and mainly for D it was. Loose lamellae may be observed even without any further calculations (such as MSDI).

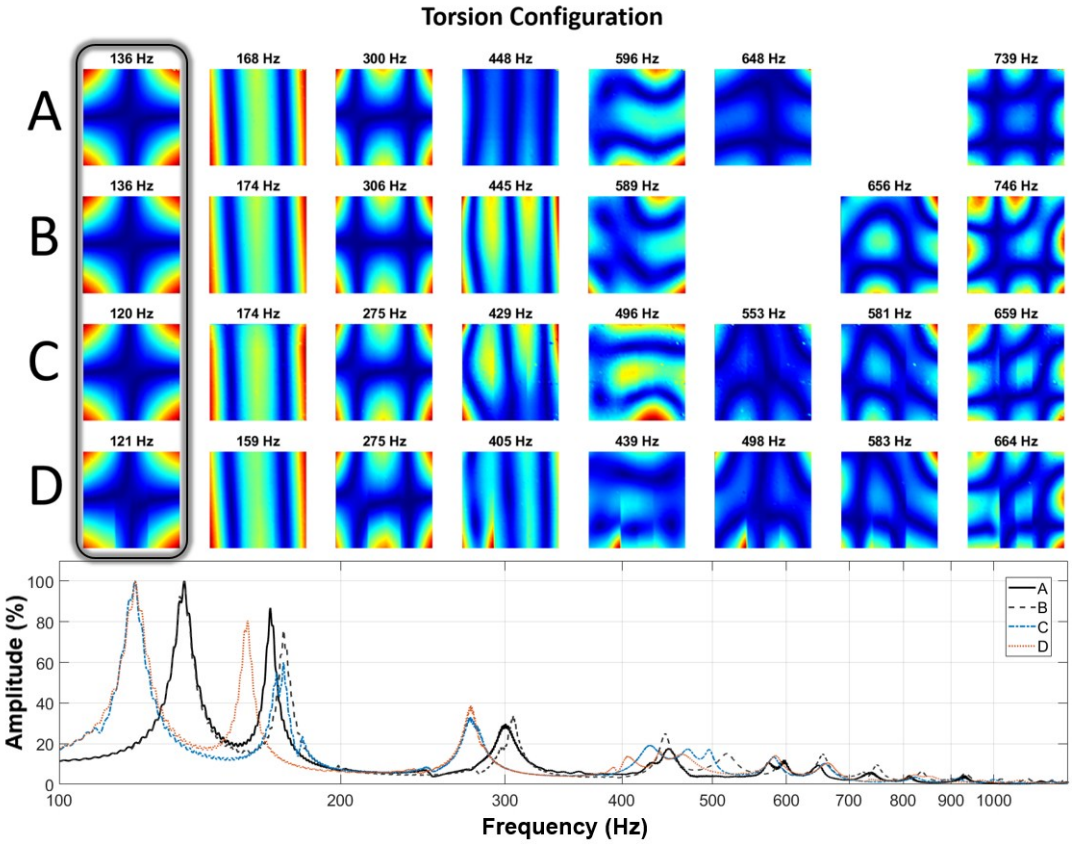

Fig. 6. Corresponding vibrational modal shapes for scenarios (A–D) and their frequencies were identified from resonance peaks in the normalised amplitude–frequency spectra obtained from the torsional measurement configuration. The torsional mode is highlighted.

If modal shapes from numerical and experimental modal analysis for torsion configuration are compared, it is apparent that the first numerical mode of 103 Hz (scenario

A) was measured to be 136 Hz, which was approx. 24 % of relative difference (RD). For scenarios B, C and D, the RD was approx. 24%, 16% and 17%, respectively. Such an RD seems to be relatively high, but one has to think that the FE model represents an ideal structure with uniform distribution of mass and stiffness, as well as ideal boundary conditions. That is likely to be a reason why numerical and experimental MA did not agree on more modal shapes for torsion configuration. Furthermore, from Fig. 6 one may also see the loose lamellae directly from modal shapes, especially for scenarios C and D. It is hypothesised that more restrained experimental boundary conditions, such as a fixed cantilever one, would lower the RD between FEA and EMA. Therefore, the next research should also focus on numerical modal analysis of CLT panels with fixed boundary conditions and with nonuniform mass and stiffness distribution that could shed more light on its effect on discrepancies between EMA and NMA.

For the configurations Bending$_L$ and Bending$_P$ (Fig. 7 and 8), one may draw similar observations as for torsional configuration: (i) the obtained eigenfrequencies decreased with damage in AB in general despite several discrepancies that may be reasoned similarly as above; (ii) bending configurations made experimental obtaining vibrational modal shapes more difficult than in case of torsion. This implies that the torsion configuration might be more suitable for the analysis of square-like CLTs on a lab level.

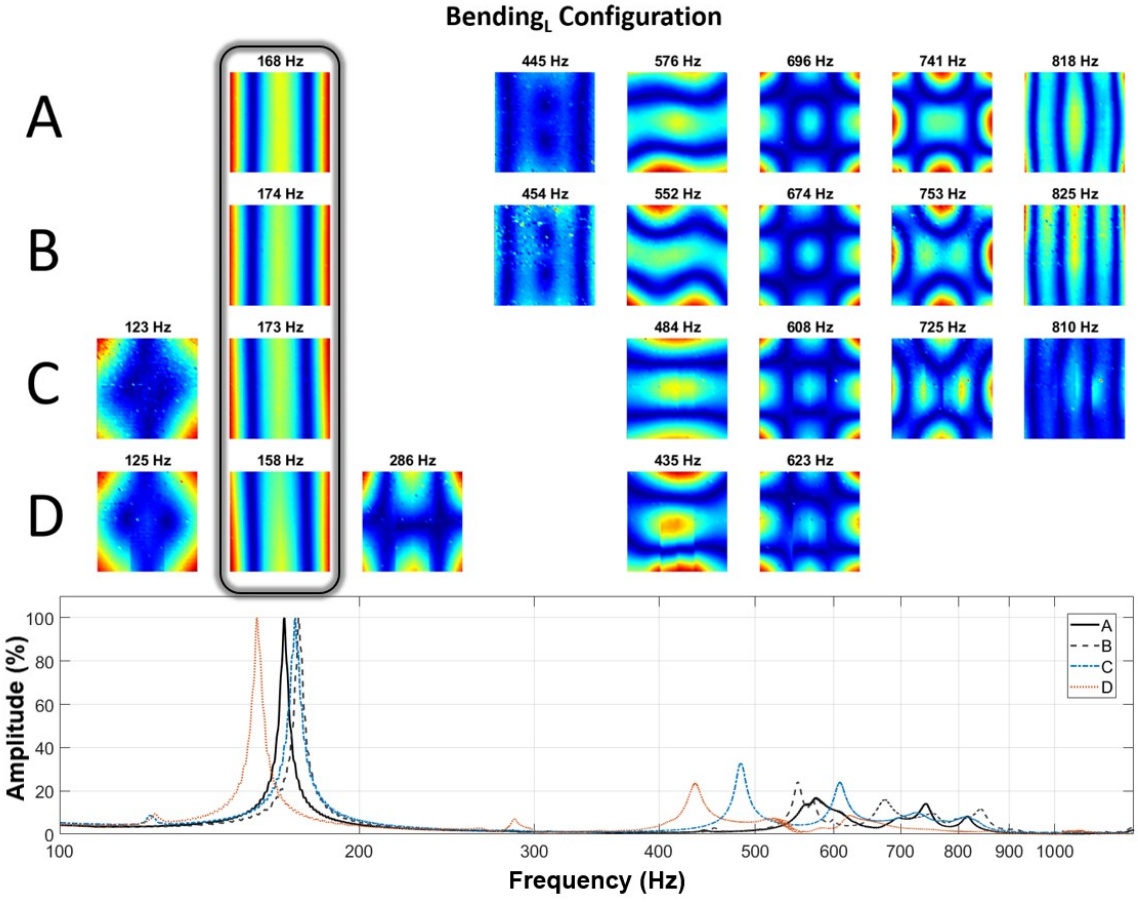

Fig. 7. Corresponding vibrational modal shapes for scenarios (A–D) and their frequencies were identified from resonance peaks in the normalised amplitude–frequency spectra obtained from the bendingL measurement configuration. The bending$_L$ mode is highlighted.

Comparison of EMA to numerical MA for configuration Bending$_L$ (Fig. 7 and S1) led to the following observations: (i) the torsional frequency obtained by EMA for C and D scenarios was not predicted by FEA for either scenario; (ii) EMA and FEA agreed on the first bending mode (highlighted in Fig. 7), the RD for A, B, C and D scenarios was 12.5%, 16.6%, 18.5%, and 6.3%, respectively; (iii) EMA and FEA further agreed on mode 11th mode in FEA (628 Hz for scenario A), experimentally matching with eigenfrequency of 696 Hz (see 6th column in Fig. 7.), its RD is 9.8%, 8%, 16.3 and 46,2% for scenarios A, B, C, and D, respectively. For scenario D, the matched mode in FEA was very likely the wrong one, not only based on its shape, but also a very low MAC that was 0.4.

Comparison of EMA to numerical MA for configuration Bending$_P$ (Fig. 8 and S2) led to the following observations: (i) the first torsional and bending frequencies obtained by EMA were not predicted by FEA for either scenario. It seems that BCs (simple supports) in FEA were still too stiff to allow these modes that are nonetheless occurring in experiments where supports are flexible ropes; (ii) EMA and FEA agreed on measured frequency 577 Hz (scenario A) that is predicted in FEM as 602 Hz, the RD for this mode is 4.3%, 6.3%, 17.8% and 42.3% for scenario A, B, C, and D, respectively. The FE-computed modes of scenarios C and D likely had wrongly assigned modes, as MAC was very low (for C and D, it was 0.41 and 0.55), which made the RD higher than for other scenarios; (iii) EMA identified the mode with f = 690 Hz (scenario A) that was computed by FE as 627 Hz, so the RD was 9.1%, 10.8%, 4.7%, and 5.9% for scenarios A, B, C, and D, respectively.

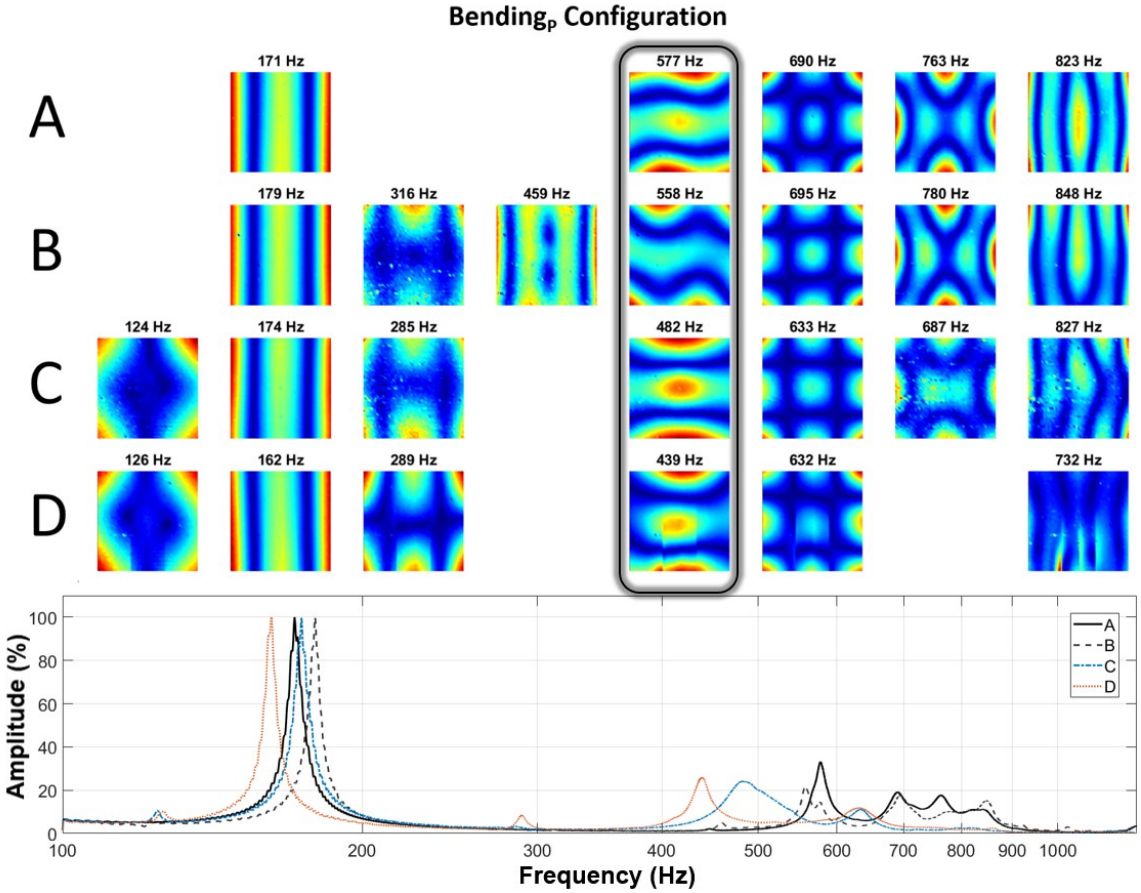

Fig. 8. Corresponding vibrational modal shapes for scenarios (A–D) and their frequencies were identified from resonance peaks in the normalised amplitude–frequency spectra obtained from the bending$_P$ measurement configuration. The bendingP mode is highlighted.

Third, the obtained spectra from EMA made it possbile to calculate damping ratios (ζ) for given scenarios and configurations. These damping ratios are listed in Table 6 and one may see the following: (i) ζ of torsion mode was higher for scenario B by 1%, for C by 22%, and for D by 25.3%; (ii) ζ of bending$_L$ was higher for B by 2.1%, for C by 18.3%, and for D by 0.7%; (iii) ζ of bending$_P$ was lower for B by 13%, and higher for C by 310.8%, and higher for D by 43.5%. Theoretically speaking, the damping ratios should increase with the increase of the damage in AB as the CLTs decrease in stiffness with damage and keep the same mass. This trend was well observable for torsional configuration and partly for configuration Bending$_P$, meanwhile for Bending$_L$, the damping held similar values except for scenario C.

Table 6. Determined Damping Ratios for the Main Modes of the Corresponding Configurations

Scenario	ζ Torsion (-)	ζ Bending$_L$ (-)	ζ Bending$_P$ (-)
A	0.0185	0.0087	0.0119
B	0.0187	0.0089	0.0103
C	0.0226	0.0103	0.0489
D	0.0232	0.0088	0.0171

Localization of Damage – FEM

The localization of the damaged AB from FEA results was carried out using MSDI, and the results may be seen in Fig. 9, 10 and 11 for Torsion, Bending$_L$, and Bending$_P$ configuration, respectively.

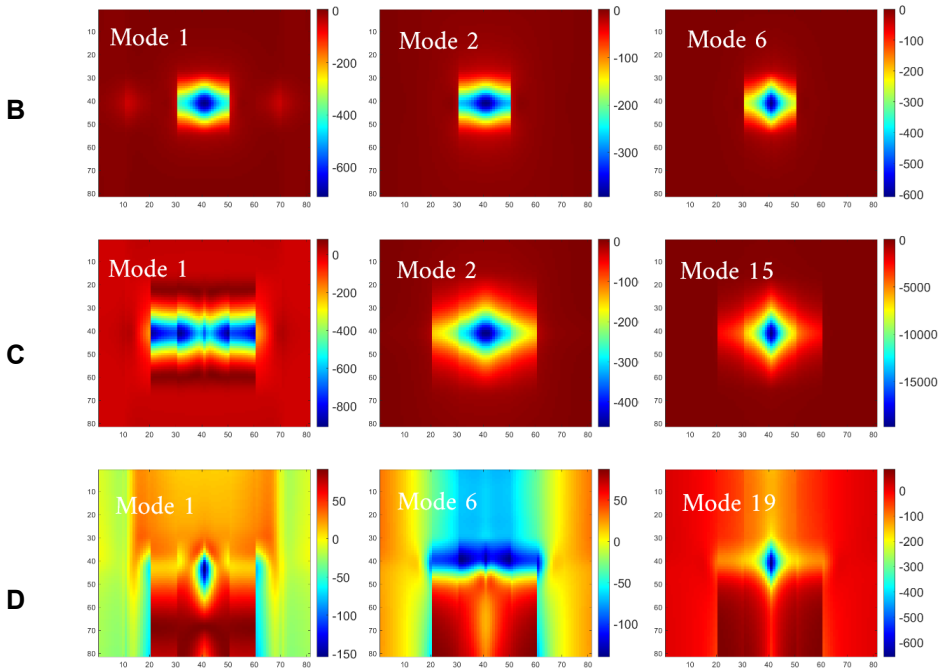

Fig. 9. MSDI computed with respect to scenario A for Torsion configuration (in %). Rows show the scenarios, and the columns express paired modes with respect to scenario A based on MAC.

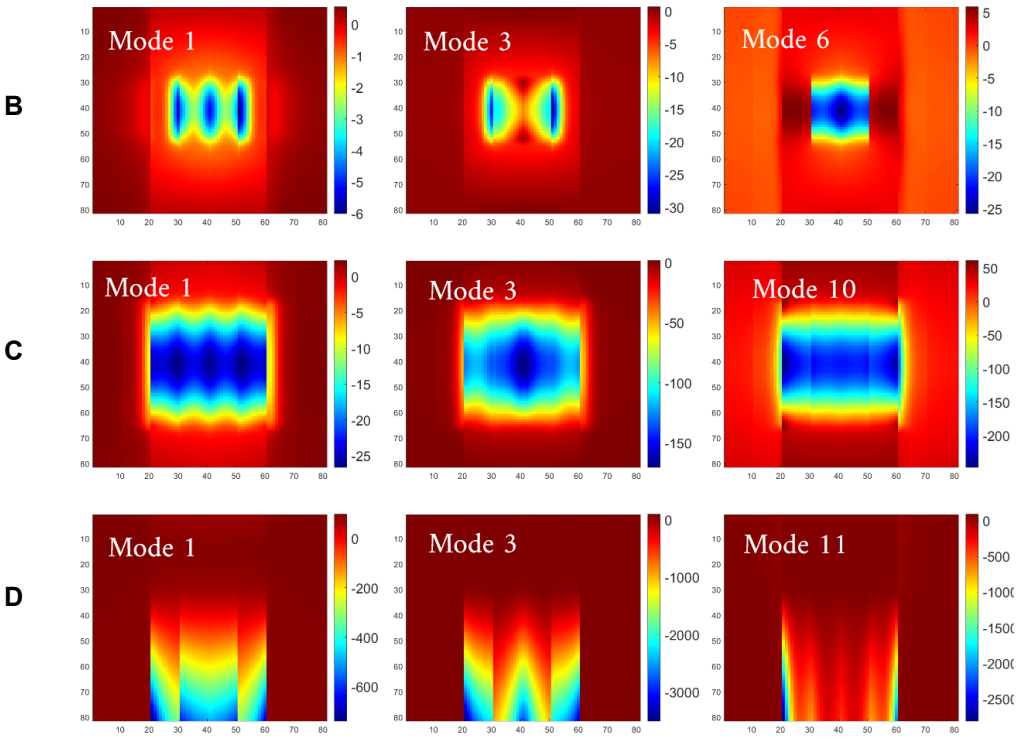

Fig. 10. MSDI computed with respect to scenario A for Bending$_L$ configuration (in %). Rows show the scenarios, and the columns express paired modes based on MAC

The subplots of Fig. 9, 10 and 11 contain the mode number as they were paired using MAC with respect to scenario A. The FEM-based MSDI for torsion configuration shows the damage in gluing very well for all extents of the damage, it is manifested as a square-like pattern easily distinguishable from the surroundings. The damage located in the center of CLT is easy to interpret; however, for scenario D, the damage is well visible not only in terms of the boundaries, but also, the edges of the individual lamellae are recognizable, for instance for MSDI of mode 19.

FE-based MSDI calculated for configuration Bending$_L$ (Fig. 10) shows that damage was well detected for all fundamental modes. For scenarios C and D, MSDI also revealed edges of particular lamellae by non-continuous contours. Since the contours were not continuous, the gradient-based scenarios could be used too to localize the damage.

FE-based MSDI calculated for configuration Bending$_P$ shows (Fig. 11) that damage was well detected, namely for scenario B. Nonetheless, for scenarios C and D, one may observe that detection of gluing damage in terms of size and shape may not be achieved for certain modes - mode 6 for scenario C and modes 34 and 7 for scenario D. These modes also have a low MAC value (≤ 0.46), so perhaps for these particular modes, the MAC may be an indicator of pairing that should not be considered valid. However, for mode 24 of scenario D, the MAC value was 0.47 and the damage was localized well in terms of shape and size. This means that MAC may be used as some kind of indicator before the calculation of MSDI, but it should be used carefully for filtering, since even for a pair with a low MAC value, the detection of glueing damage using modal displacements still might be successful.

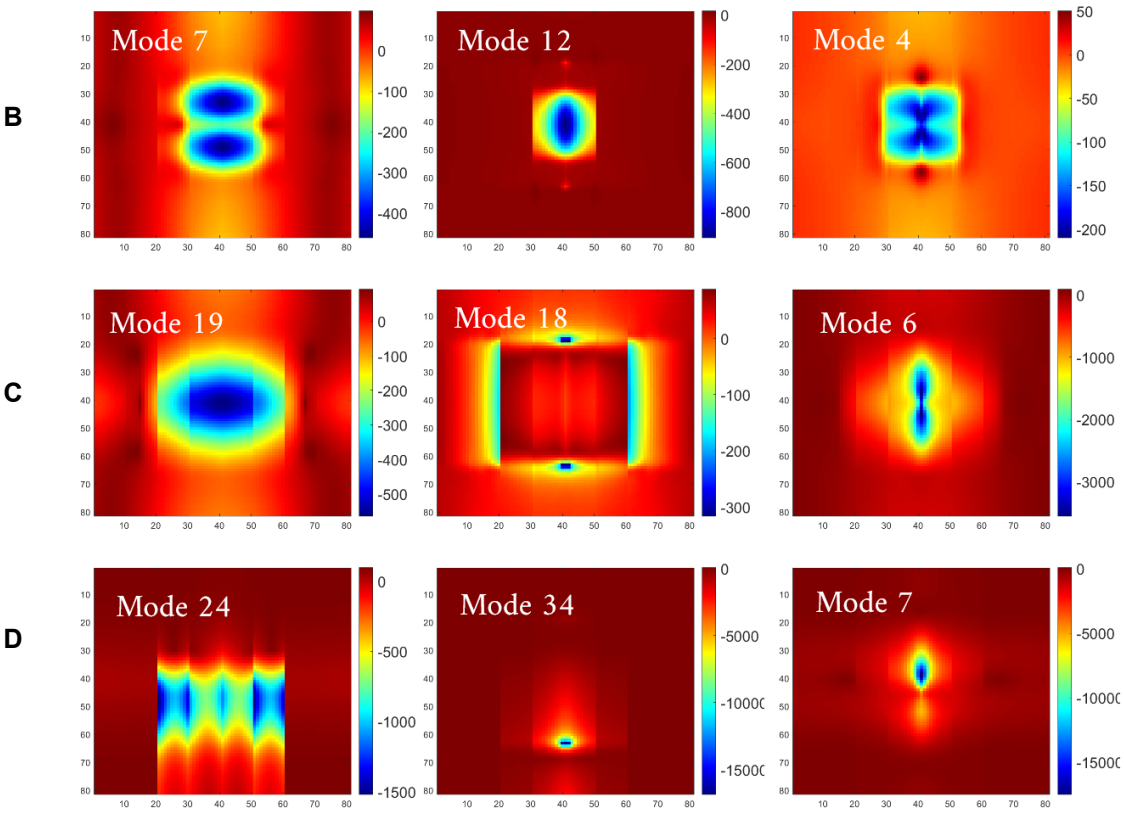

Fig. 11. MSDI computed with respect to scenario A for BendingP configuration [in %]. Rows show the scenarios, and the columns express paired modes based on MAC

Localization of Damage – Experimental

The localization of damage from experimental modal shapes was carried out in the same way as for numerical ones. The experimental modal shapes already revealed that there was damage in AB by showing the edges of loose lamellae, especially for scenarios C and D (see Fig. 6, 7, 8). Therefore, when a lamella is completely detached across its full width, its location could be identified using EMA without computing MSDI. However, this approach did not allow for localisation of the entire imperfection region in cases where only part of a lamella was unglued. The computed MSDI from modal shapes obtained by EMA calculated between the reference scenario (A) and scenarios with imperfections (B-D) are displayed in Fig. 12. In none of the cases did a high MSDI value successfully identify the known imperfection region, as was the case for FEA. In most cases, the largest discrepancies were instead found near nodal lines, so the contours of the MSDI rather copied these lines. Although the compared modal shapes were almost perfectly identical (*e.g.*, torsional or bending$_L$), subtle variations in the positioning of the nodal line within the grid of measured points—combined with the low amplitudes of nodal lines and the definition of the MSDI—were evaluated as the biggest differences we see in the Fig. 12.

To improve the MSDI results, the data were interpolated to refine the resolution, and cross-convolutions were applied to achieve the best possible alignment (even when this required shifting the meshgrid and trimming its edges). Nevertheless, nodal lines remained the highest MSDI values visible in the plots. For configurations such as bendingP or higher-order modes, the nodal lines were often very curved and varied between scenarios; in these cases, any fitting approach would not resolve the issue. The summarisation approach for the MSDI cumulation across modes did not provide any

improvement either. The idea was that imperfections could be detected by leveraging the fact that, although the largest MSDI in one mode may occur at a particular node, in another mode it would be located elsewhere, while the actual imperfection remains consistently localised. By the cumulation of these differences across multiple modes, the imperfection could emerge more clearly. However, due to the dominant MSDI values at the nodal lines and the relatively small number of available modes, this approach was unsuccessful too.

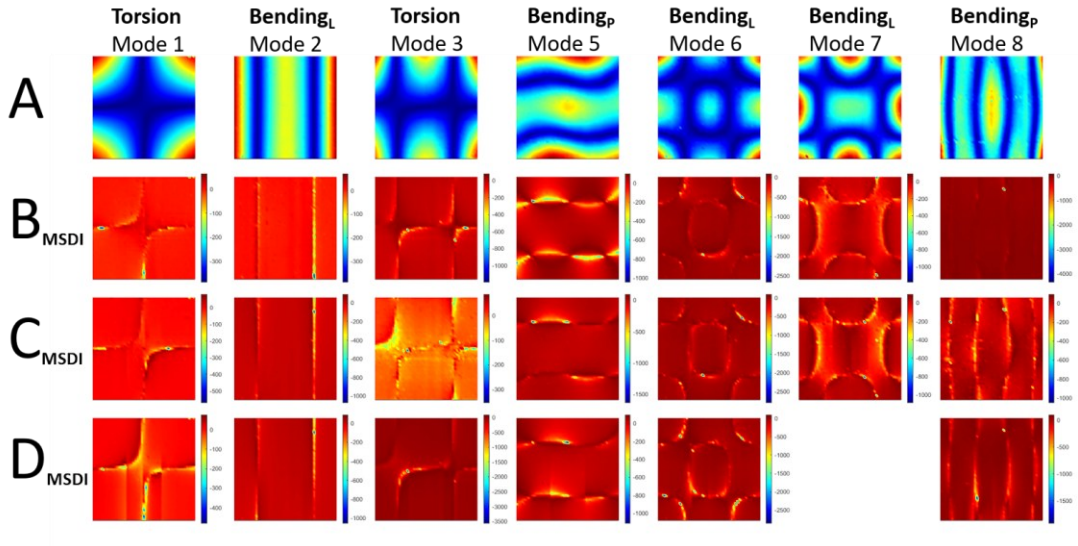

Fig. 12. Results of the modal shape damage index across modes obtained from experimental modal analysis did not markedly reveal any localisation of imperfections

The study of Duvnjak *et al*. (2021) addresses MSDI experimentally on a single concrete plate-like specimen, where the imperfect specimen is a damaged version of the reference specimen, and the measurement points remain identical. In the present study, the specimens are heterogeneous and have different mass and stiffness distributions, and although measured with high precision, the measurement points are not located at exactly the same positions, which is crucial for MSDI. This is also the reason why the procedure works for modes obtained by FEA. For experimental measurements of unique (*i.e*., non-identical) specimens, it therefore seems necessary to seek alternative approaches or to modify the experimental boundary conditions that rely on complete fixation of one side, for instance.

CONCLUSIONS

1. Experimental and numerical modal analysis may reveal damage of adhesive bonds (AB) in cross-laminated timber (CLT).
2. Damaged AB decreases main bending stiffness of the CLT, and in majority cases, it decreases eigenfrequencies, but it increases the damping coefficient. The damaged AB also introduces new modal shapes expressing motion of loose lamellae.
3. The modal assurance criterion (MAC) may be used only as one of the indicators to match CLT panels with various damages, but it should be used carefully if it is lower than 0.65-0.70.

4. The finite element method (FEM) calculated modal shapes were good input for the modal shape damage index (MSDI), as the modal shapes between scenarios may be ideally aligned – MSDI successfully identified the damage in AB, especially when calculated from fundamental modes.
5. Experimental modal analysis (EMA)-obtained modal shapes did not provide a good input for the localization of damage using MSDI, likely due to misalignment between the particular CLT panels and material properties variability within the panels.
6. To increase the success rate of application of MSDI on experimental modal shapes of CLT, it is likely necessary to have a lab setup that protects CLT against movement and has as uniform (well-sorted) wood as possible.
7. EMA showed that damage in glueing might be detectable from modal shapes directly as non-continuous contours from loose lamellae, especially if the debonding occurs for the whole width of the lamella.
8. The obtained results show a potential for in situ grading, where the primary evaluation criterion derived from EMA could be a reduction in stiffness moduli or an increase in damping coefficient, relative to the sound scenario.

ACKNOWLEDGMENTS

The work was supported by the project "Improvement and diagnostics of adhesive bondline used in multi-story timber buildings" (LUC23065) funded by the Ministry of Education, Youth and Sports of the Czech Republic.

REFERENCES CITED

Aicher, S., Dill-Langer, G. (2008). "Non-destructive detection of glue line defects in glued laminated timber," in: *10th World Conference on Timber Engineering*, 2-5 June, Japan.

Allemang, R. J. (2003). "The modal assurance criterion twenty years of use and abuse," *Sound Vib*. 37, 14-21.

Bondsman, B., and Peplow, A. (2024). "Inverse parameter identification and model updating for cross-laminated timber substructures," *J. Build. Eng*. 95, article 110209

Bondsman, B., and Peplow, A. (2025). "Experimental modal analysis and variability assessment in cross-laminated timber," *Mechanical Systems and Signal Processing* 228, article 112466, https://doi.org/10.1016/j.ymssp.2025.112466

Brandner, R., Flatscher, G., Ringhofer, A., Schickhofer, G., and Thiel, A. (2016). "Cross laminated timber (CLT): Overview and development," *Eur. J. Wood Wood Prod*. 74(3), 331-351. https://doi.org/10.1007/s00107-015-0999-5

Brown, D. L., and Allemang, R. J. (2007). "The modern era of experimental modal analysis," *Sound and Vibration* 41(1), 16-33.

Choi, F. C., Li, J., Samali, B., and Crews, K. (2007). "Application of modal-based damage-detection method to locate and evaluate damage in timber beams," *Journal of Wood Science* 53(5), 394-400. https://doi.org/10.1007/s10086-006-0881-5

Duvnjak, I., Rak, M., Damjanović, D. (2016). "A new method for structural damage detection and localization based on modal shapes," *Chapter in Life-Cycle of Engineering Systems: Emphasis on Sustainable Civil Infrastructure*, 1st Ed., CRC Press, eBook ISBN 9781315375175

Duvnjak, I., Damjanović, D., Bartolac, M., and Skender, A. (2021). "Mode shape-based damage detection method (MSDI): Experimental validation," *Appl. Sci*. 2021(11), article 4589. https://doi.org/10.3390/app11104589

Faircloth, A., Brancheriau, L., Karampour, H., So, S., Bailleres, H., and Kumar, Ch. (2021). "Experimental modal analysis of appropriate boundary conditions for the evaluation of cross-laminated timber panels for an in-line approach," *For. Prod. J.*, 71(2), 161-170.

lrretier, H. D. (2002). "History and development of frequency domain methods in experimental modal analysis," *J. Phys. IV France* 12 (2002) Pr11-91 https://doi.org/10.1051/jp4:20020480

Jarnerö, K., Brandt, A., and Olsson, A. (2015). "Vibration properties of a timber floor assessed in laboratory and during construction," *Eng. Struct*. 82, 44-54. https://doi.org/10.1016/j.engstruct.2014.10.019

Kawrza, M., Furtmüller, T., Adam, C., and Maderebner, R. (2021). "Parameter identification for a point-supported cross laminated timber slab based on experimental and numerical modal analysis," *Eur. J. Wood Wood Prod*. 79(2), 317-333. https://doi.org/10.1007/s00107-020-01641-7

Kawrza, M., Furtmüller, T., and Adam, C. (2022). "Experimental and numerical modal analysis of a cross laminated timber floor system in different construction states," *Constr. Build. Mater*. 344, no. September, p. 128032. https://doi.org/10.1016/j.conbuildmat.2022.128032

Kouroussis, G., Ben Fekih, L., and Descamps, T. (2017a). "Assessment of timber element mechanical properties using experimental modal analysis," *Construction and Building Materials* 134, 254-261. https://doi.org/10.1016/j.conbuildmat.2016.12.081

Kouroussis, G., Ben Fekih, L., and Descamps, T. (2017b). "Using experimental modal analysis to assess the behaviour of timber elements," *Mechanics & Industry* 18, article e804. https://doi.org/10.1051/meca/2017042

Kurz, J. H., and Boller, Ch. (2015). "Some background of monitoring and NDT also useful for timber structures," *Journal of Civil Structural Health Monitoring* 5(2), 99-106.

Li, S., Zeng, S., Jiang, C., Xu, G., Zhang, Z., and Sun, Q. (2023). "Damage detection of wooden beams based on the modal strain energy change and evidence theory," *BioResources* 18(3), 5133-5145.

Meruane, V., Lasen, M., López Droguett, E., and Ortiz-Bernardin, A. (2017). "Modal strain energy-based debonding assessment of sandwich panels using a linear approximation with maximum entropy," *Entropy*, 19(11), article 619. https://doi.org/10.3390/e19110619

Pahnabi, N., Schumacher, T., and Sinha, A. (2024). "Imaging of structural timber based on in situ radar and ultrasonic wave measurements: A review of the state-of-the-art," *Sensors* 24, article 2901

Pandey, A. K., Biswas, M., and Samman, M. M. (1991). "Damage detection from changes in curvature mode shapes," *Journal of Sound and Vibration* 145(2), 321-332. https://doi.org/10.1016/0022-460X(91)90595-B

Požgaj, A., Chovanec, D., Kurjatko, S., and Babiak, M. (1993). "Štruktúra a vlastnosti dreva," *Bratislava: Príroda*. ISBN 80-07-00600-1.

Roohnia, M., Manouchehri, N., Tajdini, A., Yaghmaeipour, A., and Bayramzadeh, V. (2011). "Modal frequencies to estimate the defect position in a flexural wooden beam," *BioResources* 6(4), 3676-3686. https://doi.org/10.15376/biores.6.4.3676-3686

Samali, B., Li, J., Choi, F. C., and Crews, K. (2010). "Application of the damage index method for plate-like structures to timber bridges," *Struct. Control Health Monit*. 17, 849-871.

Shi, J., Yin, S., Huang, W., and Na, B. (2025). "Application of vibrational methods in wood performance testing: A short review," *BioResources* 20(2), 4861-4876. https://doi.org/10.15376/biores.20.2.4861-4876

Song, S. Q., Xu, H. D., and Wang, L. H. (2011). "The application of modal analysis in hole-defect in lumber," *Key Engineering Materials*, 467-469. https://doi.org/10.4028/www.scientific.net/KEM.467-469.1776

Ussher, E., Arjomandi, K., Weckendorf, J., and Smith, I. (2017), "Predicting effects of design variables on modal responses of CLT floors," *Structures* 11, 40-48. https://doi.org/10.1016/j.istruc.2017.04.006

Wang, F. L., and Chan, T. H. T. (2009). "Review of vibration-based damage detection and condition assessment of bridge structures using structural health monitoring," in: *The Second Infrastructure Theme Postgraduate Conference: Rethinking Sustainable Development: Planning, Engineering, Design and Managing Urban Infrastructure*; Queensland University of Technology: Brisbane, Australia, pp. 35-47.

Weckendorf, J., Ussher, E., and Smith, I. (2016). "Dynamic response of CLT plate systems in the context of timber and hybrid construction," *Compos. Struct.* 157, 412-423. https://doi.org/10.1016/j.compstruct.2016.08.033

Yang, X., Ishimaru, Y., Iida, I., and Urakami, H. (2002). "Application of modal analysis by transfer function to nondestructive testing of wood I: Determination of localized defects in wood by the shape of the flexural vibration wave," *J. Wood Sci*. 48(4), 283-288.

Yang, X., Amano, T., Ishimaru, Y., and Iida, I. (2003). "Application of modal analysis by transfer function to nondestructive testing of wood II: Modulus of elasticity evaluation of sections of differing quality in a wooden beam by the curvature of the flexural vibration wave," *J. Wood Sci*. 49(2), 140-144.

Article submitted: September 4, 2025; Peer review completed: October 5, 2025; Revised version received: December 1, 2025; Accepted: March 19, 2026; Published: April 17, 2026.
DOI: 10.15376/biores.21.2.4830-4853

APPENDIX

Supplemental Material S1 - Bending$_L$

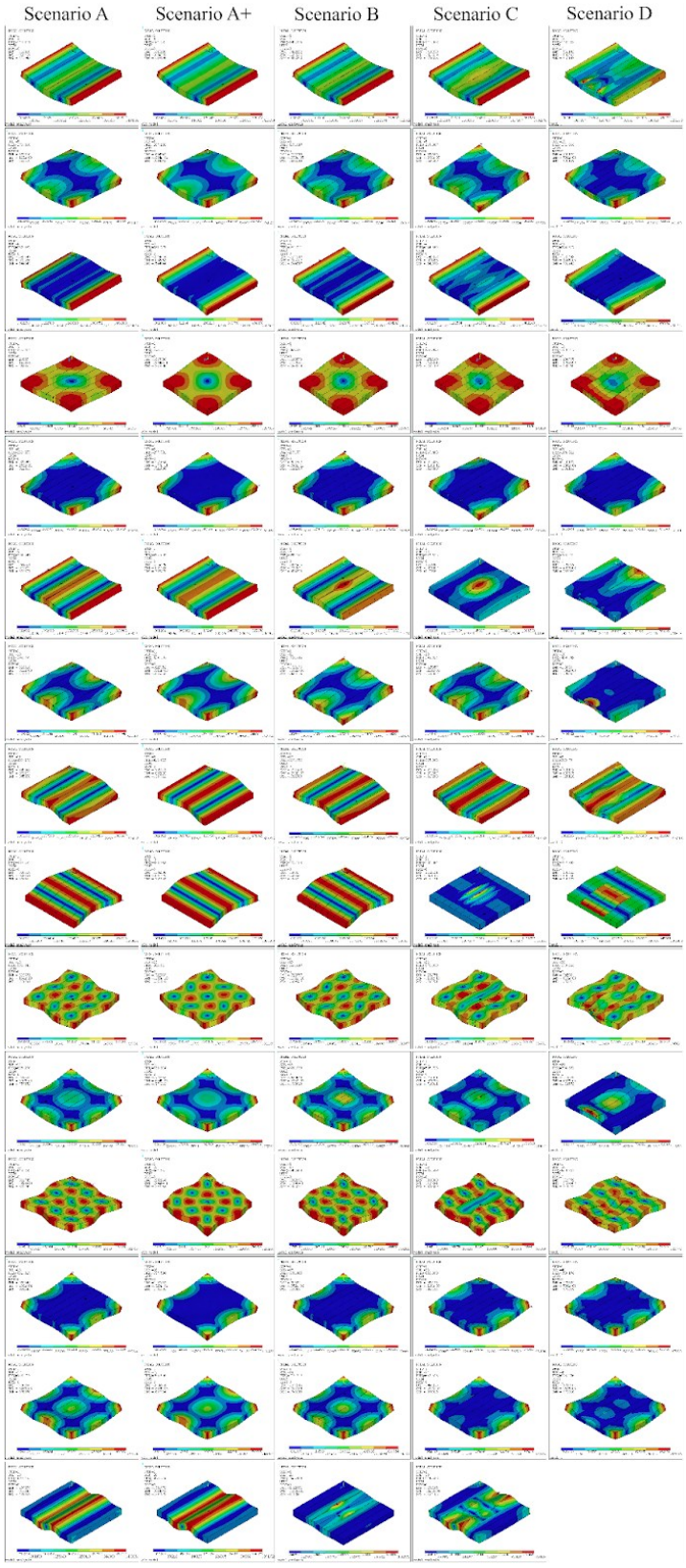

Supplemental Material S2 - Bending$_P$

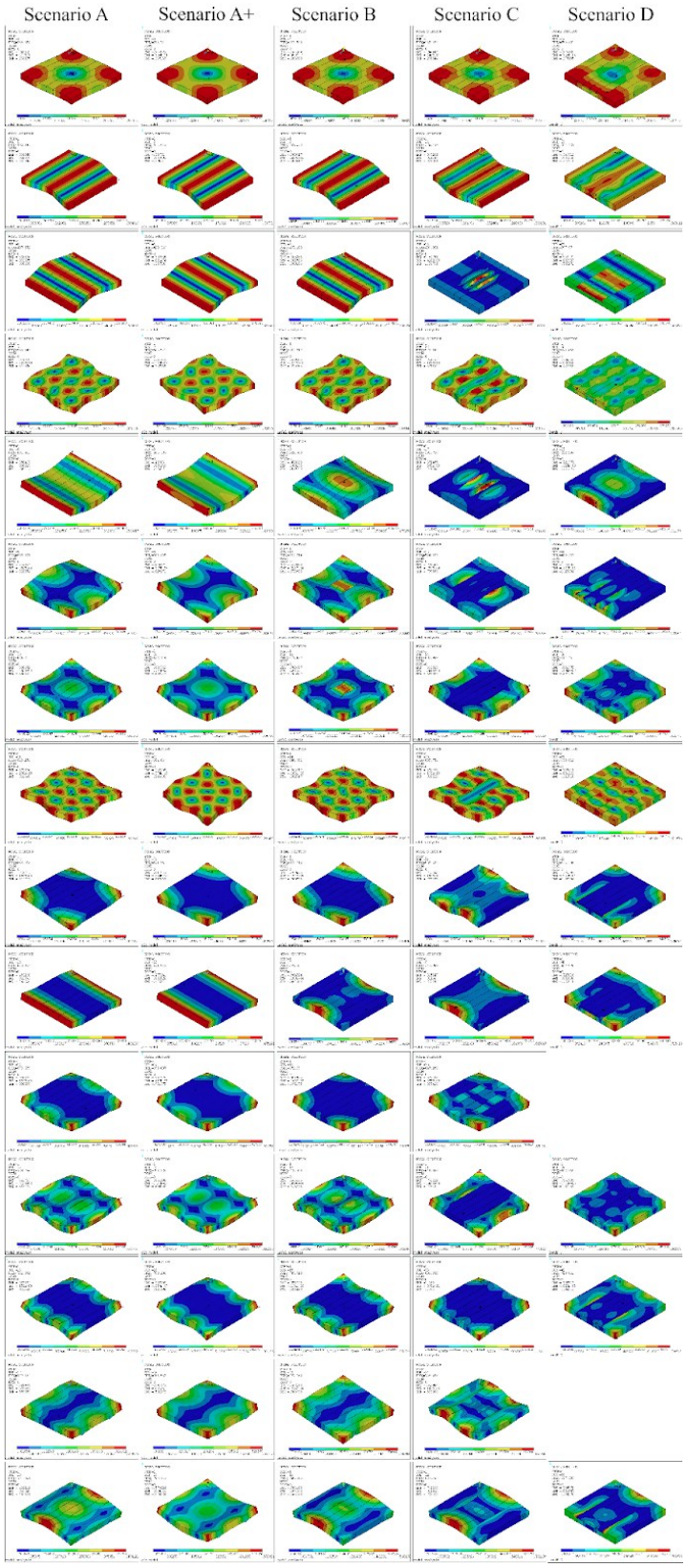

Supplemental Material S3 – Torsion